nature chemical biology

ARTICLES

https://doi.org/10.1038/s41589-020-0509-x

Check for updates

Topology-dependent interference of synthetic gene circuit function by growth feedback

Rong Zhang[1,3], Jiao Li[1,2,3], Juan Melendez-Alvarez[1], Xingwen Chen[1], Patrick Sochor[1], Hanah Goetz[1], Qi Zhang[1], Tian Ding[2], Xiao Wang[1]✉ and Xiao-Jun Tian[1]✉

Growth-mediated feedback between synthetic gene circuits and host organisms leads to diverse emerged behaviors, including growth bistability and enhanced ultrasensitivity. However, the range of possible impacts of growth feedback on gene circuits remains underexplored. Here we mathematically and experimentally demonstrated that growth feedback affects the functions of memory circuits in a network topology-dependent way. Specifically, the memory of the self-activation switch is quickly lost due to the growth-mediated dilution of the circuit products. Decoupling of growth feedback reveals its memory, manifested by its hysteresis property across a broad range of inducer concentration. On the contrary, the toggle switch is more refractory to growth-mediated dilution and can retrieve its memory after the fast-growth phase. The underlying principle lies in the different dependence of active and repressive regulations in these circuits on the growth-mediated dilution. Our results unveil the topology-dependent mechanism on how growth-mediated feedback influences the behaviors of gene circuits.

Circuit–host interactions affect behaviors of synthetic gene circuits, thereby adding an additional layer of complexity to already intricate gene regulatory networks[1–3]. There are many sources of circuit–host interactions, including metabolic burden[4,5], cell growth[6–8] and resource relocation/competition[9–12]. These interactions are often neglected in the design of gene circuits by assuming that gene circuits are generally orthogonal to the host background[13–16]. In many instances, however, the effects of circuit–host interactions are substantial[17–19]. Understanding the mechanisms of how circuit–host interactions are established, particularly the effects of these interactions on gene circuit functions, will help us to better formulate control strategies for designing and engineering robust gene circuits.

Various feedback loops are created by circuit–host interactions. For example, growth feedback is formed given that the expression of synthetic gene circuits inevitably causes metabolic burden to host cells and thus affects cell growth, which in turn changes gene expression of circuits[8,20]. This growth feedback endows gene circuits with various emerged properties, including enhanced ultrasensitivity[21,22], innate growth bistability[23] and toxin cooperativity[24]. However, the desired functions of gene circuits also can be attenuated by growth feedback.

Here, we studied how the network topology affects the extent to which growth feedback influences the memory maintenance function of synthetic switch circuits. Several different topologies can be used to create a bistable switch, including a toggle switch or self-activation (SA) switch[25–31]. Previously, it was theoretically predicted that the SA or toggle switch would be differently regulated by growth feedback under constant growth rate conditions[8,20]. To test the hysteresis properties of these switches, one dilution protocol was often used to ensure cells in the exponential growth phase. For example, in the seminal work of the toggle switch, all the samples were diluted in fresh medium every 6–10 h (ref. [25]). The underlying reason is that cell growth can be maintained at a relatively constant rate. While this dilution protocol works successfully to demonstrate the hysteresis behavior, an important question naturally arises concerning whether bistable behavior can be observed robustly in conditions where the growth rate is rather dynamic.

Here, we systematically tested the dynamics of two bistable switches under various cell growth conditions. We found that the memory of the SA switch is lost due to cell growth, and thus no hysteresis was found using the dilution protocol with fresh medium. However, after uncoupling growth feedback from gene circuits, we found a broad range of bistability. On the contrary, the toggle switch is more refractory to growth feedback. We demonstrated the underlying mechanism using mathematical modeling and theoretical analysis by integrating the dynamics of cell growth into the gene circuits. Thus, we concluded that the effects of growth-mediated feedback on gene circuits depend on their network topologies.

Results

Inconsistent in silico and in vivo analysis of SA circuit. To determine the effects of growth feedback on gene circuits, we first built a simple SA circuit, in which the transcriptional factor AraC forms a dimer and binds to promoter P_{bad} in the presence of stimulus L-(+)-arabinose (L-ara), which in turn activates the expression of itself and the reporter green fluorescent protein (GFP). We measured the dose–response curve of promoter P_{bad}, which shows ultrasensitivity after parameter fitting (Fig. 1a). Based on the fitted parameters, we developed a mathematical model for the SA circuit (see Supplementary Note for details) and predicted that the SA circuit is bistable. As shown in Fig. 1b, the system switches from 'OFF' to 'ON' once the stimulus level reaches above the threshold and stays in the ON state even if the stimulus is removed.

To test our prediction, we measured the response of the SA circuit with varying doses of L-ara. Clear bimodal distributions were observed in a broad range of L-ara concentrations (Fig. 1c), with some cells in a GFP^{high} state and others in a GFP^{low} state, suggesting the system could be bistable. Further experiments were conducted to test the hysteresis behavior. First, initially OFF cells were treated with a series dose of L-ara for 17 h, and the fraction of ON cells was measured by flow cytometry, which shows a switch behavior

[1]School of Biological and Health Systems Engineering, Arizona State University, Tempe, AZ, USA. [2]Department of Food Science and Nutrition, Zhejiang University, Hangzhou, Zhejiang, China. [3]These authors contributed equally: Rong Zhang, Jiao Li. ✉e-mail: xiaowang@asu.edu; xiaojun.tian@asu.edu

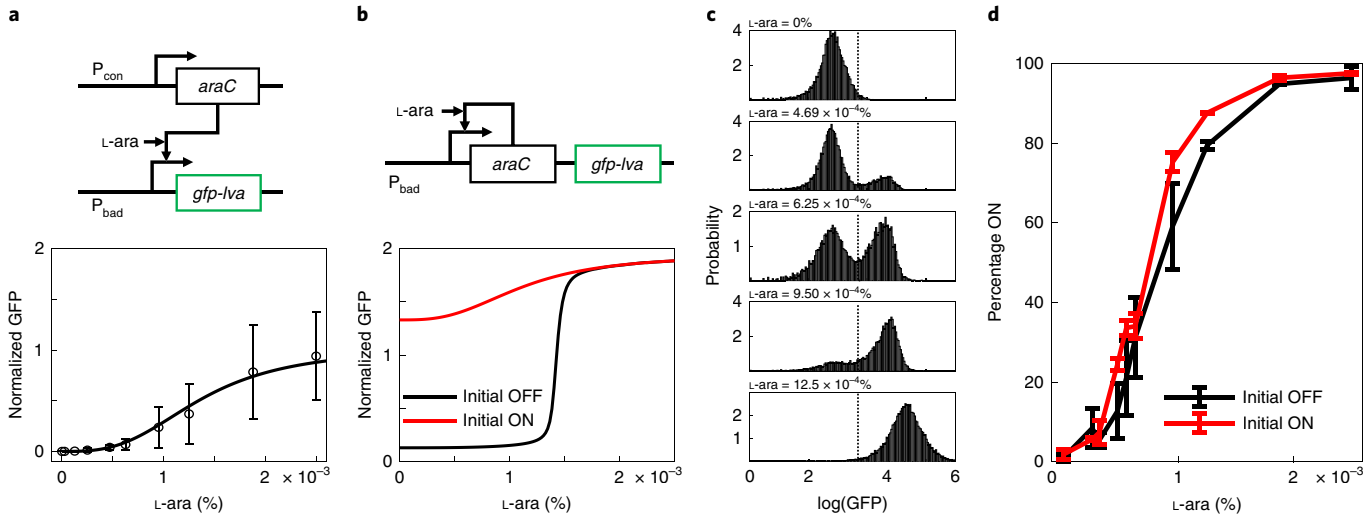

Fig. 1 | Theoretical analysis reveals bistability, but experimental data shows no hysteresis. a, Parameter fitting the dose–response curve of the promoter (P_{bad}) shows ultrasensitivity. The results show mean ± s.d. ($n = 6$). Constitutive promoter (P_{con}) was used to express AraC. Unstable GFP variant (GFP-lva) was used as the reporter. **b**, Mathematical model predicts bistability from the SA circuit with P_{bad} promoter. **c**, Steady-state distribution of GFP after 17 h induction of various doses of L-ara with the initial state OFF shows two distinct states (separated by the dash lines), ON and OFF. **d**, The steady-state fraction of ON cells after 17- to 18-h induction of L-ara with the initial state OFF or ON shows no hysteresis. The ON cells were pretreated with a high dose of L-ara (2.5×10^{-3}%). Data displayed as mean ± s.d. ($n = 3$).

(Fig. 1d, black line). Second, ON cells (pretreated with high-dose L-ara) were diluted into fresh medium with various concentrations of L-ara. After 18 h, the ON cells fraction showed a curve similar to the one without pretreatment (Fig. 1d, red line), which was confirmed by the similar steady-state GFP curves (Supplementary Fig. 1). Thus, seemingly inconsistent conclusions are drawn between theoretical prediction and experimental verification.

Growth feedback disguises bistability of SA circuit. To uncover the underlying reason for this inconsistency, we further studied the temporal dynamics of ON cells. After diluting the ON cells into fresh media with various concentrations of L-ara, the cell density (measured as optical density (OD) at 600 nm) and GFP fluorescence were measured at different time points. We observed that cell growth slowed down as the population reached the carrying capacity, following the logistic model (Fig. 2a). However, the average GFP level (GFP/OD) decreased rapidly during the exponential growth phase and reached a very low level 3 h after dilution (Fig. 2b), indicating the memory loss of the circuit. Later, GFP started accumulating and then reached different steady states depending on L-ara levels (Fig. 2b) and generated curves similar to the ones started from the OFF state cells (Supplementary Fig. 2). It is important to note that the GFP level maintained well for 6 h after the cells reached the stationary phase. To exclude potential factors associated with the stationary phase for memory loss, cells activated by high dose of L-ara to different levels of GFP at different OD (~0.3–0.7) were diluted into fresh medium with high-dose or no L-ara. As shown in Supplementary Fig. 3, GFP in all the samples showed a decline after dilution, consistent with the results of the stationary phase cells (Fig. 2b). Similar phenomena were also observed in the LuxR SA circuit (Supplementary Fig. 4). To investigate whether the dilution frequency contributes to memory loss, we studied GFP dynamics after dilution of ON cells every 3 or 6 h into fresh medium with high-dose or without L-ara. As shown in Supplementary Fig. 5, the dynamics of GFP were the same as the case without frequent dilutions (Fig. 2b) when the ON cells were diluted into no L-ara fresh medium. This suggests that memory loss is not affected by the dilution frequency. When the ON cells were diluted into high-dose L-ara fresh medium, the GFP level always decreased to the lowest point after each dilution (Supplementary Fig. 5). Thus, the memory loss of the SA circuit could result from dilution of gene circuit products by fast cell growth where the dilution frequency does not contribute to its memory loss.

We also found that the cell growth rate decreased while the gene expression level of the SA circuit increased (Supplementary Fig. 6), which is consistent with previous findings that synthetic circuits cause burdens to the cells and inhibit cell growth[6,8,21,32]. Consequently, the memory loss of the SA circuit could arise from the outgrowth of ON-state cells by OFF-state cells at the population level[33]. To study whether the growth rate heterogeneity among cells contributes to the memory loss here, we first conducted stochastic simulations at the single-cell level (see Supplementary Note for details) in three scenarios including (1) WT with both growth rate heterogeneity and growth-mediated dilution, (2) growth-mediated dilution only and (3) growth rate heterogeneity only. As shown in Supplementary Fig. 7, while in scenario 2 the circuit lost the memory at a similar speed as it did in scenario 1 (Supplementary Fig. 7a,b and blue/red curves in Supplementary Fig. 7d), the memory loss was very slow in scenario 3 (Supplementary Fig. 7c and yellow curve in Supplementary Fig. 7d), which was not consistent with our experimental data (Fig. 2b). We then conducted an experiment by mixing various fractions of OFF cells into ON cells and measured the GFP dynamics to compare the speed of memory loss. As shown in Supplementary Fig. 7e,f, the curves of GFP dynamics demonstrated a similar speed of memory loss, even though the memory loss was slightly faster for the samples with more OFF cells. Thus, we conclude that the memory loss mainly resulted from growth-mediated dilution despite the fact that growth rate heterogeneity also contributed to it.

All these data suggest the existence of a feedback loop between the synthetic gene circuit and the cell growth, in which the gene expression of circuit slows down cell growth, whereas fast cell growth dilutes the gene expression (Fig. 2c). To further understand how cell growth changes circuit behavior, we revised our mathematical model by integrating growth feedback (see Supplementary Note for details). We conducted a simulation to demonstrate how the SA

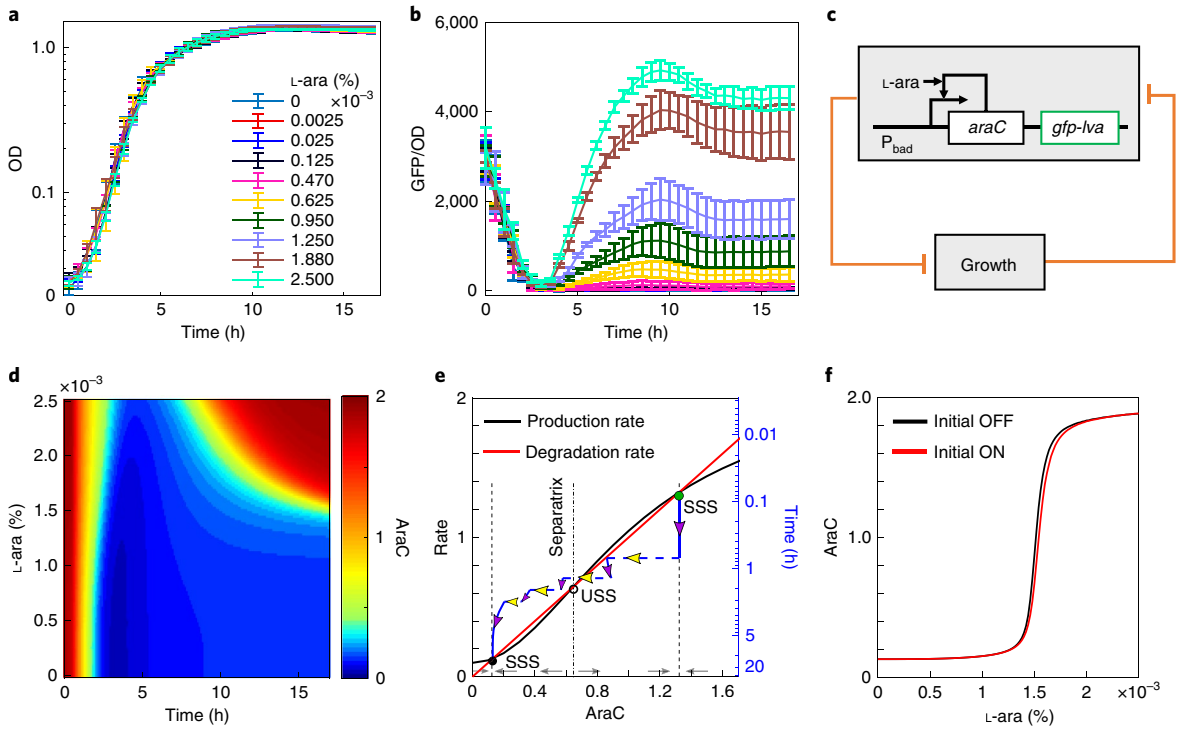

Fig. 2 | Growth-mediated feedback disguises the bistability of the SA circuit. a,**b**, Dynamics of growth (OD) (**a**) and GFP/OD (**b**) after 1:100 dilution of ON cells into fresh medium with various doses of L-ara. Data indicate mean ± s.d. ($n = 3$). **c**, Diagram of coupling gene circuit with cell growth. The mathematical model is revised based on this diagram. **d**, Simulation with revised mathematical model shows AraC level as a function of time and L-ara dose. The system was set to ON state initially. **e**, The process of memory loss of the SA circuit. Simulated trajectory (blue lines) of one cell is shown on the rate-balance plot of AraC. Two SSSs (solid circles) and one USS (open circle) are shown at the intersection of the production rate curve and degradation curve. The system was set to the ON state initially (solid green circle) and L-ara was set to 0. Four cell division events were considered in simulation (dashed line with yellow arrow). The separatrix (dash-dotted line) determines whether the system goes to ON or OFF states directed by the gray arrows. The rate-balance plot is based on the model without growth feedback. **f**, Simulation confirms that the bistable range of the SA circuit is significantly reduced when coupled with growth feedback.

circuit lost its memory. At the population level, a full range of AraC dynamics under different levels of L-ara is shown in Fig. 2d. Initially, AraC was set at a high level but decreased very quickly to low levels, consistent with the experimental results (Fig. 2b). At the single-cell level, we used the algorithm by considering the stochasticity from cell divisions before the system reaches the stationary phase (see Supplementary Note for details). Two stable steady states (SSSs) and one unstable steady state (USS) can be found at the intersections of the production and degradation rates of AraC (Fig. 2e). The AraC level was set to high level in the ON state (solid green circle in Fig. 2e) initially, and then decreased because of cell division-mediated dilution (blue dashed lines with yellow arrows in Fig. 2e), and later started to accumulate (solid blue lines with purple arrows in Fig. 2e) because of AraC production by the SA circuit. However, the dilution was much faster than the accumulation, and thus AraC levels decreased very quickly to a point that was below the separatrix (dash-dotted line in Fig. 2e) and converged to the OFF state (solid black circle in Fig. 2e), and was maintaining in this state even after the cell growth slowed down in the prestationary phase and stopped in the stationary phase. That is, at the early stage, the growth feedback was dominant and continuously diluted the circuit products, leading to the switching-off of the circuit. This is the underlying mechanism for the memory loss of the SA circuit and the reason why no hysteresis was found using the dilution protocol with fresh media (Figs. 1d and 2f).

For theoretical analysis, we also considered a scenario of constant growth rate to study how the strength of growth feedback affects the gene circuits (see Supplementary Note for details). Increasing the growth rate indeed changes the bifurcation diagram significantly (Supplementary Fig. 8a). The activation threshold of the switch increases quickly with the growth rate (Supplementary Fig. 8b). This suggests that it is unlikely to activate the system with the experiment under fast-growth conditions. Taken together, growth feedback disguises the bistable property of the SA circuit.

Decoupling growth feedback shows bistability of SA circuit. These results showed that dilution with the fresh medium can keep cells fast-growing, but inevitably it induces the growth feedback to synthetic gene circuits, leading to memory loss. To decouple growth feedback from circuits and overcome this detrimental effect, we developed a new dilution protocol by diluting cells into the conditioned medium collected from stationary phase culture (Supplementary Fig. 9a). To test this protocol, the activated cells were first loaded into a microfluidic platform and fresh medium with or without L-ara was provided. We found that the GFP level was extinguished quickly along with several cell divisions regardless of L-ara levels (Fig. 3a,b and Supplementary Videos 1 and 2), thereby confirming the memory loss of the SA circuit due to the growth feedback (Fig. 2b). After switching to the conditioned medium, we observed that the GFP level did not recover without L-ara (Fig. 3a and Supplementary Video 1) but elevated under high-dose L-ara (Fig. 3b and Supplementary Video 2), which is consistent with Fig. 2b. Furthermore, we measured the system dynamics under conditioned medium at the population level. We found that cells did not divide as OD was maintained in low level (Fig. 3c and Supplementary Fig. 9b) but still had a strong ability to express the

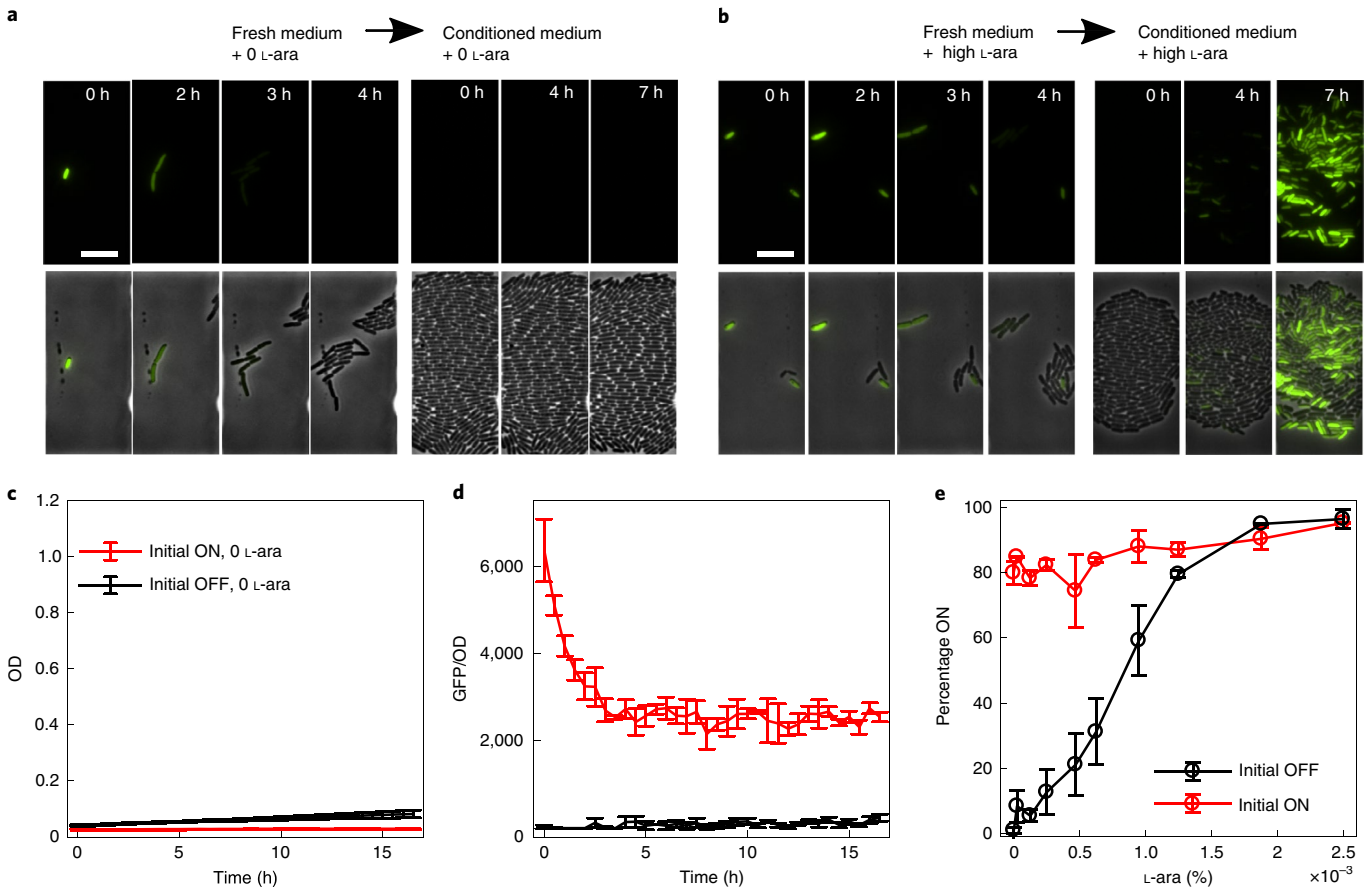

Fig. 3 | Decoupling of growth feedback reveals the bistability of the SA circuit. a,**b**, Time-lapse imaging of GFP (and brightfield overlay) in the SA circuit showed that it switches off after several rounds of cell divisions with fast growth in fresh medium and then did not recover in the conditioned medium without inducer (**a**) but recovered with high-dose L-ara (**b**). Representative results from three replicates are shown. Scale bars, 10 μm. **c**,**d**, The dynamics of growth (**c**) and GFP (**d**) after 1:100 dilution of ON cells into the conditioned medium without L-ara. Negative control (black line) was the OFF cells grown in conditioned medium with no L-ara. **e**, Hysteresis curves obtained using the new protocol by diluting ON cells into the conditioned medium with various doses of L-ara. Data indicate mean ± s.d. ($n = 3$).

genes of the circuit since the GFP levels were well maintained during 17 h for all L-ara concentrations (Fig. 3d and Supplementary Fig. 9c). It is noted that the maintenance of GFP is not from its slow degradation as unstable GFP variant (GFP-lva)[34] with a half-life of 68 min is used in the circuit (Supplementary Fig. 10). This is consistent with the observed findings of a surprisingly long period of constant protein production activity in the stationary phase of bacteria[35]. Finally, a very large range of hysteresis was revealed (Fig. 3e), indicating that the system actually functions as an irreversible bistable switch, consistent with the prediction in Fig. 1b. These data suggest that growth feedback can be decoupled under slow or nongrowth conditions. To further confirm this, we diluted the activated cells into low nutrition medium M9 with either no or high-dose L-ara. The memory was maintained very well in both cases of low nutrition medium (Supplementary Fig. 11a), in contrast with the samples diluted in high nutrition medium (Supplementary Fig. 11b). Taken together, decoupling growth feedback with conditioned medium or with low-nutrient medium helps maintain circuit memory and reveals the bistability of the SA circuit.

Toggle switch is refractory to growth feedback. To study whether the growth feedback also affects other types of gene circuit, we tested our protocol with the toggle switch, in which two genes *TetR* and *LacI* inhibit each other. In the original work, cells were diluted into fresh medium frequently to maintain cells in the log growth phase[25]. The hysteresis behavior of the toggle switch was indeed found. However, the effects of growth feedback on the toggle switch are unclear. Thus, we studied the dynamics of the toggle switch with our protocols. At the population level, after dilution of activated cells into fresh medium, which couples the growth feedback with the toggle switch circuit (Fig. 4a), GFP levels decreased to the minimum at 4 h after dilution (Fig. 4b,c and Supplementary Fig. 12a,b). However, the GFP level was retrieved for all samples with various doses of inducer anhydrotetracycline hydrochloride (aTc), indicating that the memory of the toggle switch was maintained during the fast-growth phase and can be retrieved in the slow-growth phase. Similarly, after dilution of ON cells into conditioned medium to decouple growth feedback, GFP levels were also well maintained for 17 h (Supplementary Fig. 12c,d). The GFP maintenance is not from its slow degradation as unstable GFP variant (GFP-laa), which has a similar half-life to GFP-lva, was used in the circuit[34,36].

At the single-cell level using microfluidics, GFP level decreased with cell division in the fresh medium regardless of aTc doses and increased after switching to the conditioned medium both with or without aTc (Supplementary Fig. 12e,f and Supplementary Videos 3 and 4), which is consistent with Fig. 4c. The system needed more time to recover without aTc (Supplementary Fig. 12e and Supplementary Video 3) in contrast to high dose aTc (Supplementary Fig. 12f and Supplementary Video 4). In Fig. 4d, the hysteresis curves from both conditioned medium (black curve) and fresh medium (red curve)

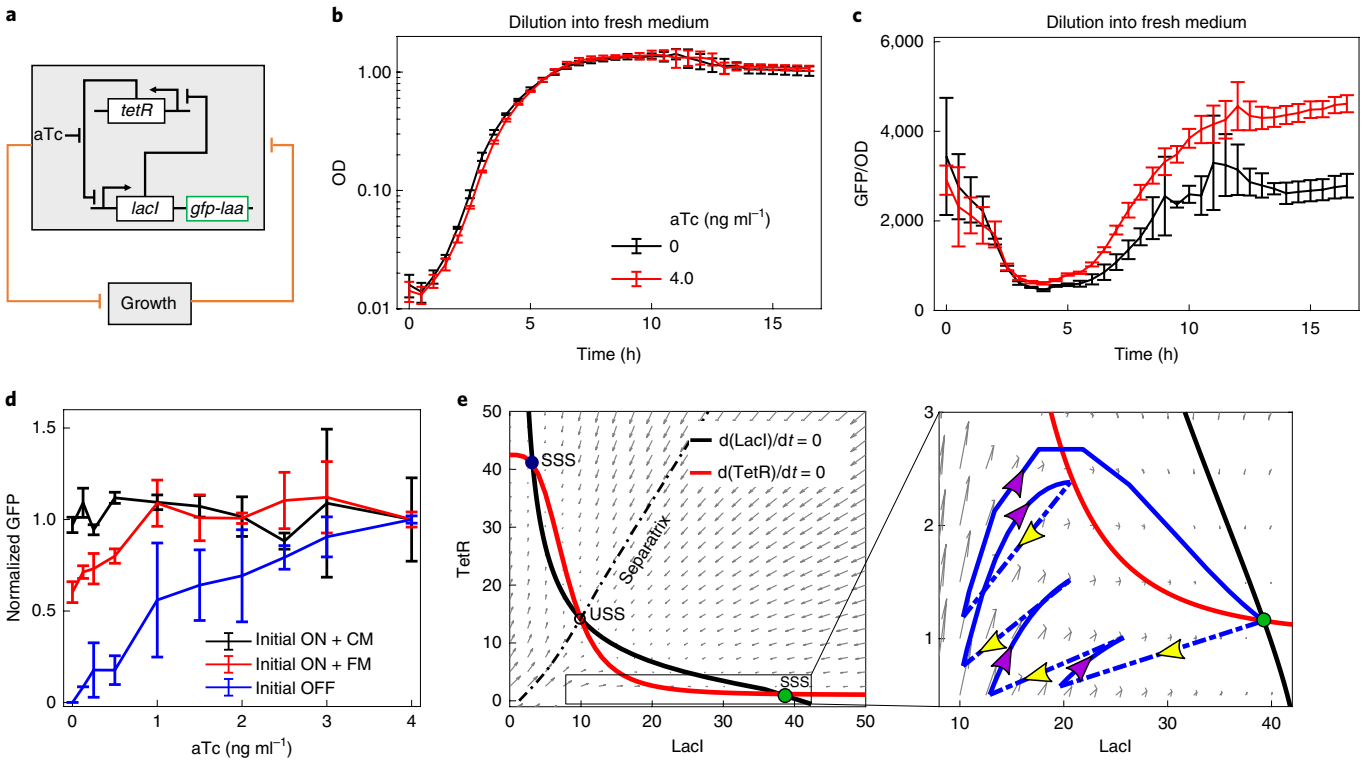

Fig. 4 | The toggle switch is refractory to memory loss from the growth-mediated feedback. a, Diagram of the toggle switch circuit coupled with growth feedback. Unstable GFP variant (GFP-laa) is used as the reporter. **b**,**c**, Dynamics of OD (**b**) and GFP (OD) (**c**) after 1:100 dilution of ON cells into fresh medium with high-dose or without inducer aTc. **d**, Hysteresis curves with conditioned medium (CM, black curve) and fresh medium (FM, red curve). GFP level was normalized to the level at the highest aTc. **e**, Simulated trajectory (blue lines) of one cell is shown in the direction field of LacI/TetR. Four cell division events were considered (indicated by dashed lines with yellow arrows in the enlarged box area). Two SSSs (solid circles) and one USS (open circle) are shown at the intersection of nullclines (defined as the derivations of LacI and TetR equal to 0 with respect to time t (d(LacI)/dt = 0 and d(TetR)/dt = 0), black and red curves). The system was set to the ON state initially (solid green circle) and aTc was set to 0. The separatrix (dash-dotted line) determines whether the system goes to the ON or OFF state directed by the gray arrows. The nullcline curves were based on the model without growth feedback. Data indicate mean ± s.d. (n = 3).

showed the irreversibility of the toggle switch, consistent with the previous works[25,37,38]. Thus, the toggle switch is refractory to memory loss from growth feedback.

To study how the topology differs for the response of the SA circuit and the toggle switch to growth feedback, similar simulations were performed to analyze the toggle switch's behavior. First, at the population level, no difference was found in the hysteresis curves for fast growth and no growth conditions (Supplementary Fig. 13), consistent with experimental results (Fig. 4d). At the single-cell level, the trajectory of one cell is shown to demonstrate how the system changes with several cell divisions and then recovers to the original state. As shown in the directed field for the toggle switch (Fig. 4e), two SSSs and one USS can be found at the intersections of the nullclines. The cell was set initially in the $LacI^{High}/TetR^{Low}$ state (ON state, solid green circle in Fig. 4e) and then moved toward the bottom-left corner (Fig. 4e, blue dashed lines with yellow arrows) due to cell division. The system tried to recover toward the top-right corner (Fig. 4e, solid blue lines with purple arrows) after each cell division. After several rounds of competition between accumulation and growth-mediated dilution, the system reached a stationary growth phase but was still in the domain where it can easily recover to the original state. We further compared the robustness of these two bistable switches to the growth-mediated effect in terms of timescale. As shown in Supplementary Fig. 14, if the timescale of the SA circuit is fast enough that it has a chance to recover to the original state after each cell division, it maintains its memory and is robust to cell growth (Supplementary Fig. 14a). That is, the SA circuit can maintain its memory theoretically, although it is impossible to build such a gene circuit with super-fast dynamics since transcription and translation always take time for any gene circuits. The toggle switch gene circuit is more robust in general if the timescales of LacI and TetR are balanced (Supplementary Fig. 14b). If the timescales of two genes are not well balanced with relatively slow TetR timescale, the system is still robust to the cell division Supplementary Fig. 14c), while it could be sensitive to cell division if the LacI timescale is significantly slow (Supplementary Fig. 14d). That is, the toggle switch maintains its memory in a much broader timescale range than the SA circuit. Taken together, the toggle switch circuit is more robust in general to the growth-mediated dilution than the SA circuit.

The main differences between the SA circuit and toggle switch are the gene promoters used in the circuits. The promoter P_{bad} in the SA circuit is positively regulated by AraC, while promoter P_{Tet} in the toggle switch is negatively regulated by TetR. Given that the activity of promoter P_{bad} directly depends on AraC concentration, the dilution of AraC significantly decreases its production rate in the SA circuit. While the activity of promoter P_{Tet} inversely depends on TetR concentration, the dilution of TetR does not decrease the relative production rates of the two genes in the circuit and thus leads to robust memory (Supplementary Fig. 15). These differences between the toggle switch and SA circuit are also reflected in the directions of the dilution (dashed lines with the yellow arrows in Fig. 2e and Fig. 4e). The dilution direction is more parallel to the

separatrix for the toggle switch (dash-dotted line in Fig. 4e), while it is perpendicular to the separatrix for the SA circuit (dash-dotted line in Fig. 2e). This is the reason why the system has crossed the separatrix after two cell divisions for the SA circuit, while it still has not crossed the separatrix after four cell divisions for the toggle switch. In summary, the network topology of the toggle switch makes it robust to growth feedback.

Discussion

It is still a big challenge to build large-sized synthetic gene circuits since circuits often do not function as expected once they are assembled. One fundamental reason is that multiple factors of circuit–host interactions, such as metabolic burden, cell growth feedback and resource competition, are often neglected when building and testing gene circuits because of the assumption that the circuits are orthogonal to the host background. However, we know that physiological links from host to gene circuits create a hidden regulatory layer, which often perturbs the expected functions of gene circuits. In addition, it is difficult to predict how these hidden interactions affect circuit functions and how we can minimize unfavorable effects. Our data suggest that the circuit–host interaction mediated by growth feedback may disguise the true behavior of gene circuits. The interference depends on the network topology of gene circuits. While the SA circuit is sensitive to growth feedback and loses its memory easily, the toggle switch circuit is robust to growth feedback and can maintain its memory very well even though some decline has been found due to fast cell growth. In retrospect, this results from different dependencies of simple negative and positive regulations on growth rate[8]. The expression of target gene increases with the growth rate for a negative regulation but decreases for a positive regulation[8]. Given that most synthetic gene circuits are composed of simple negative and positive regulations, the circuit–host interactions affect each link differently and thus can significantly change gene circuits functions. Furthermore, it will be interesting to study how the noise associated with growth-related fluctuations in global gene expression affects the behavior of the circuits given that the noise level is coupled with the growth rate[39]. The analysis of input-associated signed activation time can be used in designing robust switches[40,41].

Here, we found that growth feedback has an adverse effect on the functions of some gene circuits as the memory can be lost due to fast cell growth. Previously, it has also been found that growth feedback can lend new properties to other gene circuits. A constitutively expressed antibiotic resistance gene, for example, shows innate growth bistability given that the expression of the resistance gene is growth-dependent and the cell growth is modulated by translation-targeting antibiotics[23]. It is also reported that growth feedback makes some other circuit systems more cooperative[8,21]. A noncooperative circuit, autoregulation of T7 RNA polymerase, was found to generate bistability unexpectedly[21]. The underlying mechanism is that the nonlinear dilution of T7 RNA polymerase induced by growth feedback enhances overall effective cooperativity. Our results are consistent with this work, as an increase in growth rate indeed expands the bistable range (Supplementary Fig. 8). In the case of the autoregulation of T7 RNA polymerase, the circuit itself is not bistable, but the nonlinear dilution introduced by growth feedback increases the circuit ultrasensitivity and makes it bistable. In the case of the SA circuit here, it is bistable when growth feedback is decoupled. However, under the conditions of constant growth rate with frequent dilution into the fresh medium, the activation threshold increases so quickly that the switch's activation is infeasible in the biologically reasonable range. Thus, the effect of interactions between the circuit and the host is double-edged. While they endow new properties to some gene circuits, they impair or disguise the desired behaviors of others. Controlling strategies should be developed for the latter case. In this paper, we present a strategy by controlling the growth rate to minimize the effects of growth feedback on memory circuits. We found that conditioned medium from the stationary phase or fresh medium with minimal nutrients can be used to slow down the growth rate and thus maintain the memory of the circuits. This is also consistent with previous work that a surprisingly long period of constant protein production activity during the stationary phase of bacteria was reported[35].

We demonstrated how the growth feedback affects the memory maintenance of two memory gene circuits and the underlying mechanism of how the SA circuit is susceptible to growth feedback, while the toggle switch is robust. The primary factor is the perturbated concentrations of transcription activators and repressors due to cell growth, which cause the promoter activity changes of the circuits. Our results indicate that the changes in gene activity during the fast cell growth phase due to the resource allocation strategy of cells during their division. That is, resources such as ATP, as well as transcriptional and translational machinery components, are biased toward cell–cell-driven changes[42]. One strategy to control this uncertainty is to integrate the synthetic gene circuits into the genome of the cell[43]. Another method is to manipulate the size of resource pools[44,45]. Orthogonal ribosome pools or orthogonal DNA replication systems have been used to alleviate the effect of resource competition and gene coupling[46–48]. Insulation-based engineering strategies have shown to improve the resolution of the genetic circuit[49]. Future work is needed to further understand mechanisms of how circuit–host interactions affect gene circuits and to develop corresponding control strategies for robust gene circuits.

Online content

Any Nature Research reporting summaries, source data, extended data, supplementary information, acknowledgements, peer review information; details of author contributions and competing interests; and statements of data and code availability are available at https://doi.org/10.1038/s41589-020-0509-x.

Received: 27 August 2019; Accepted: 28 February 2020;
Published online: 06 April 2020

References

1. Brophy, J. A. & Voigt, C. A. Principles of genetic circuit design. *Nat. Methods* **11**, 508–520 (2014).
2. Liao, C., Blanchard, A. E. & Lu, T. An integrative circuit-host modelling framework for predicting synthetic gene network behaviours. *Nat. Microbiol.* **2**, 1658–1666 (2017).
3. Boo, A., Ellis, T. & Stan, G.-B. Host-aware synthetic biology. *Curr. Opin. Syst. Biol.* **14**, 66–72 (2019).
4. Lynch, M. & Marinov, G. K. The bioenergetic costs of a gene. *Proc. Natl Acad. Sci. USA* **112**, 15690–15695 (2015).
5. Ceroni, F. et al. Burden-driven feedback control of gene expression. *Nat. Methods* **15**, 387–393 (2018).
6. Scott, M., Gunderson, C. W., Mateescu, E. M., Zhang, Z. & Hwa, T. Interdependence of cell growth and gene expression: origins and consequences. *Science* **330**, 1099–1102 (2010).
7. Weisse, A. Y., Oyarzun, D. A., Danos, V. & Swain, P. S. Mechanistic links between cellular trade-offs, gene expression, and growth. *Proc. Natl Acad. Sci. USA* **112**, E1038–E1047 (2015).
8. Klumpp, S., Zhang, Z. & Hwa, T. Growth rate-dependent global effects on gene expression in bacteria. *Cell* **139**, 1366–1375 (2009).
9. Qian, Y., Huang, H. H., Jimenez, J. I. & Del Vecchio, D. Resource competition shapes the response of genetic circuits. *ACS Synth. Biol.* **6**, 1263–1272 (2017).
10. Erickson, D. W. et al. A global resource allocation strategy governs growth transition kinetics of *Escherichia coli*. *Nature* **551**, 119–123 (2017).
11. Venturelli, O. S. et al. Programming mRNA decay to modulate synthetic circuit resource allocation. *Nat. Commun.* **8**, 15128 (2017).
12. Klumpp, S. & Hwa, T. Growth-rate-dependent partitioning of RNA polymerases in bacteria. *Proc. Natl Acad. Sci. USA* **105**, 20245–20250 (2008).
13. Lu, T. K., Khalil, A. S. & Collins, J. J. Next-generation synthetic gene networks. *Nat. Biotechnol.* **27**, 1139–1150 (2009).
14. Purnick, P. E. & Weiss, R. The second wave of synthetic biology: from modules to systems. *Nat. Rev. Mol. Cell Biol.* **10**, 410–422 (2009).
15. Kwok, R. Five hard truths for synthetic biology. *Nature* **463**, 288–290 (2010).

16. Purcell, O., Jain, B., Karr, J. R., Covert, M. W. & Lu, T. K. Towards a whole-cell modeling approach for synthetic biology. *Chaos* **23**, 025112 (2013).
17. Cardinale, S. & Arkin, A. P. Contextualizing context for synthetic biology–identifying causes of failure of synthetic biological systems. *Biotechnol. J.* **7**, 856–866 (2012).
18. Zhang, C., Tsoi, R. & You, L. Addressing biological uncertainties in engineering gene circuits. *Integr. Biol. Quant. Biosci. Nano Macro* **8**, 456–464 (2016).
19. Arkin, A. P. A wise consistency: engineering biology for conformity, reliability, predictability. *Curr. Opin. Chem. Biol.* **17**, 893–901 (2013).
20. Klumpp, S. & Hwa, T. Bacterial growth: global effects on gene expression, growth feedback and proteome partition. *Curr. Opin. Biotechnol.* **28**, 96–102 (2014).
21. Tan, C., Marguet, P. & You, L. Emergent bistability by a growth-modulating positive feedback circuit. *Nat. Chem. Biol.* **5**, 842–848 (2009).
22. Nevozhay, D., Adams, R. M., Van Itallie, E., Bennett, M. R. & Balazsi, G. Mapping the environmental fitness landscape of a synthetic gene circuit. *PLoS Comput. Biol.* **8**, e1002480 (2012).
23. Deris, J. B. et al. The innate growth bistability and fitness landscapes of antibiotic-resistant bacteria. *Science* **342**, 1237435 (2013).
24. Feng, J., Kessler, D. A., Ben-Jacob, E. & Levine, H. Growth feedback as a basis for persister bistability. *Proc. Natl Acad. Sci. USA* **111**, 544–549 (2014).
25. Gardner, T. S., Cantor, C. R. & Collins, J. J. Construction of a genetic toggle switch in *Escherichia coli*. *Nature* **403**, 339–342 (2000).
26. Lou, C. et al. Synthesizing a novel genetic sequential logic circuit: a push-on push-off switch. *Mol. Syst. Biol.* **6**, 350–350 (2010).
27. Isaacs, F. J., Hasty, J., Cantor, C. R. & Collins, J. J. Prediction and measurement of an autoregulatory genetic module. *Proc. Natl Acad. Sci. USA* **100**, 7714–7719 (2003).
28. Wu, F., Su, R. Q., Lai, Y. C. & Wang, X. Engineering of a synthetic quadrastable gene network to approach Waddington landscape and cell fate determination. *eLife* **6**, e23702 (2017).
29. Zeng, W. et al. Rational design of an ultrasensitive quorum-sensing switch. *ACS Synth. Biol.* **6**, 1445–1452 (2017).
30. Li, T. et al. Engineering of a genetic circuit with regulatable multistability. *Integr. Biol. Quant. Biosci. Nano Macro* **10**, 474–482 (2018).
31. Wu, F., Menn, D. J. & Wang, X. Quorum-sensing crosstalk-driven synthetic circuits: from unimodality to trimodality. *Chem. Biol.* **21**, 1629–1638 (2014).
32. Dong, H., Nilsson, L. & Kurland, C. G. Gratuitous overexpression of genes in *Escherichia coli* leads to growth inhibition and ribosome destruction. *J. Bacteriol.* **177**, 1497–1504 (1995).
33. Blanchard, A. E., Liao, C. & Lu, T. Circuit-host coupling induces multifaceted behavioral modulations of a gene switch. *Biophys. J.* **114**, 737–746 (2018).
34. Andersen, J. B. et al. New unstable variants of green fluorescent protein for studies of transient gene expression in bacteria. *Appl Environ. Microbiol.* **64**, 2240–2246 (1998).
35. Gefen, O., Fridman, O., Ronin, I. & Balaban, N. Q. Direct observation of single stationary-phase bacteria reveals a surprisingly long period of constant protein production activity. *Proc. Natl Acad. Sci. USA* **111**, 556–561 (2014).
36. Litcofsky, K. D., Afeyan, R. B., Krom, R. J., Khalil, A. S. & Collins, J. J. Iterative plug-and-play methodology for constructing and modifying synthetic gene networks. *Nat. Methods* **9**, 1077–1080 (2012).
37. Menn, D., Sochor, P., Goetz, H., Tian, X. J. & Wang, X. Intracellular noise level determines ratio control strategy confined by speed-accuracy trade-off. *ACS Synth. Biol.* **8**, 1352–1360 (2019).
38. Wu, M. et al. Engineering of regulated stochastic cell fate determination. *Proc. Natl Acad. Sci. USA* **110**, 10610–10615 (2013).
39. Keren, L. et al. Noise in gene expression is coupled to growth rate. *Genome Res.* **25**, 1893–1902 (2015).
40. Wang, L., Xin, J. & Nie, Q. A critical quantity for noise attenuation in feedback systems. *PLoS Comput. Biol.* **6**, e1000764 (2010).
41. Chen, M., Wang, L., Liu, C. C. & Nie, Q. Noise attenuation in the ON and OFF states of biological switches. *ACS Synth. Biol.* **2**, 587–593 (2013).
42. Slager, J. & Veening, J. W. Hard-wired control of bacterial processes by chromosomal gene location. *Trends Microbiol* **24**, 788–800 (2016).
43. Moon, T. S., Lou, C., Tamsir, A., Stanton, B. C. & Voigt, C. A. Genetic programs constructed from layered logic gates in single cells. *Nature* **491**, 249 (2012).
44. Zhong, Z., Ravikumar, A. & Liu, C. C. Tunable expression systems for orthogonal DNA replication. *ACS Synth. Biol.* **7**, 2930–2934 (2018).
45. Liu, C. C., Jewett, M. C., Chin, J. W. & Voigt, C. A. Toward an orthogonal central dogma. *Nat. Chem. Biol.* **14**, 103–106 (2018).
46. Arzumanyan, G. A., Gabriel, K. N., Ravikumar, A., Javanpour, A. A. & Liu, C. C. Mutually orthogonal DNA replication systems in vivo. *ACS Synth. Biol.* **7**, 1722–1729 (2018).
47. Darlington, A. P. S., Kim, J., Jimenez, J. I. & Bates, D. G. Dynamic allocation of orthogonal ribosomes facilitates uncoupling of co-expressed genes. *Nat. Commun.* **9**, 695 (2018).
48. An, W. & Chin, J. W. Synthesis of orthogonal transcription-translation networks. *Proc. Natl Acad. Sci. USA* **106**, 8477–8482 (2009).
49. Zong, Y. et al. Insulated transcriptional elements enable precise design of genetic circuits. *Nat. Commun.* **8**, 52 (2017).

Methods

Strains, media and chemicals. *Escherichia coli* DH10B (Invitrogen) was used for all the cloning construction experiments. Measurement of the self-activated circuit was performed in *E. coli* K-12 MG1655ΔlacIΔaraCBAD as described in ref. [28]. Measurement of the toggle switch was performed with *E. coli* K-12 MG1655ΔlacI as described in ref. [37]. Cells were grown in 5 ml or 15 ml tubes with 220 rotations per minute at 37 °C in Luria-Bertani medium (LB medium) with 100 μg ml^{-1} chloramphenicol or 50 μg ml^{-1} kanamycin. L-ara (Sigma-Aldrich) and aTc (Abcam) were dissolved in ddH_2O and later diluted to appropriate working solution.

Plasmids construction. The AraC SA circuit was constructed into either a pSB1C3 (high copy number, used for flow cytometry and plate reader analysis) or pSB3K3 (medium copy number, used for microfluidics) backbone according to the standard molecular cloning protocols using the standardized BioBricks parts from the iGEM Registry (https://igem.org/registry). The LuxR SA circuit was constructed into a pSB1C3 backbone. The *araC* gene was amplified by PCR using the BioBrick part BBa_C0080 as the template to have the lva-tag removed. The primers used were forward 5′-ctggaattcgcggccgcttctagatggctgaagcgcaaaatgatc-3′ and reverse 5′-ggactgcagcggccgctactagtagtttattatgacaacttgacggctacatc-3′. The BioBricks used were BBa_B0034 (ribosome binding site, RBS), BBa_K206000 (P_{bad}), BBa_K145015 (GFP with lva-tag), BBa_B0015 (transcriptional terminator) and BBa_C0062 (LuxR). The sequence of pLux is 5′-acctgtaggatcgtacagggttacgcaagaaaatggtttgttatagtcgaataaa-3′. pLux was amplified by PCR using the BioBrick part BBa_R0062 as template. The primers used were forward 5′-gcttctagagacctgtaggatcgtacagggttacgcaagaaaatggtttgttatag-3′ and reverse 5′- ggactgcagcggccgctactagtatttattcgactataacaaaccattttc-3′. Detailed characterization of pLux can be found on website http://parts.igem.org/Part:BBa_R0062. All parts were first restriction digested using desired combinations of two FastDigest restriction enzymes chosen from EcoRI, XbaI, SpeI and PstI (Thermo Fisher), separated by gel electrophoresis and then purified using GelElute Gel Extraction Kit (Sigma-Aldrich) followed by ligation using T4 DNA ligase (New England BioLabs). Then the ligation products were transformed into *E. coli* strain DH10B and later the positive colonies were screened. Finally, the plasmids were extracted using GenElute Plasmids Miniprep Kit (Sigma-Aldrich) and verified by sequencing. The operons constituting the SA circuits were constructed monocistronically. The plasmid of the toggle switch was kindly provided by J. Collins as described in refs. [37,38].

Hysteresis experiment. For the hysteresis experiment using conditioned medium, on day 1, plasmids carrying the SA circuit were transformed into *E. coli* K-12 MG1655ΔlacIΔaraCBAD. The transformants were then spread onto a LB agar plate with 100 μg ml^{-1} chloramphenicol and were grown at 37 °C overnight. In the morning of day 2, one colony was inoculated into 200 μl LB with 100 μg ml^{-1} chloramphenicol and was grown in a 5 ml culture tube on a shaker for about 6 h to reach stationary phase. Then 4 μl of the cells were inoculated into in 4 ml LB medium with 100 μg ml^{-1} chloramphenicol and were grown on a shaker at 37 °C overnight using 15 ml culture tubes with or without induction. For the induction of the SA circuit, 2.5×10^{-3}% L-arabinose (L-ara) was added to the growth medium. An identical culture without arabinose was grown in parallel. In the morning on day 3, the cells had reached the stationary phase, and the cultures were centrifuged (2,000*g* for 5 min) and supernatant from the parallel culture without L-ara was sterile-filtered and was used as the conditioned medium. For flow cytometry and plate reader analysis, the pellet from L-ara containing culture was first washed twice with conditioned medium without L-ara; then the resuspended cells were diluted 100-fold into culture tubes containing 1 ml conditioned medium with different concentrations of L-ara added (OD of the cells was around 0.02 measured in 200 μl volume by plate reader). Finally, the cells were incubated in the shaker and measured at indicated time points for flow cytometry, or loaded onto a 96-well plate for plate reader analysis. Hysteresis experiment using the conditioned medium for the toggle switch was performed the same way with the induction switched to aTc.

For the hysteresis experiment using fresh medium, on day 1, plasmids carrying the SA circuit were transformed into *E. coli* K-12 MG1655ΔlacIΔaraCBAD. The transformants were then spread onto a LB agar plate with 100 μg ml^{-1} chloramphenicol and were grown at 37 °C overnight. In the morning of day 2, one colony was inoculated into 200 μl LB with 100 μg ml^{-1} chloramphenicol and was grown in a 5 ml culture tube on a shaker for about 6 h to reach the stationary phase. Then, 4 μl of the cells were then inoculated into in 4 ml LB medium with 100 μg ml^{-1} chloramphenicol and were grown on a shaker at 37 °C overnight using 15 ml culture tubes with or without induction. For the induction of the SA circuit, 2.5×10^{-3}% L-ara was added to the growth medium. In the morning of day 3, the cultures were centrifuged (2,000*g* for 5 min) and the pellet was first washed twice with warm LB without L-ara; then the resuspended cells were diluted 100-fold into culture tubes containing 1 ml fresh medium with different concentrations of L-ara added (OD of the cells was around 0.02 measured in 200 μl volume by plate reader). Finally, the cells were incubated in the shaker and measured at indicated time points for flow cytometry, or loaded onto a 96-well plate for plate reader analysis. Hysteresis experiment using fresh medium for the toggle switch was performed the same way with the induction switched to aTc.

Flow cytometry. All samples were analyzed using Accuri C6 flow cytometer (Becton Dickinson) with excitation/emission filters 480 and 530 nm (FL1-A) for GFP detection at indicated time points. For each sample, 10,000 events were recorded. At least three replicated tests were performed for each experiment. Data files were analyzed with MATLAB (MathWorks).

Dynamic analysis performed by Plate Reader. Synergy H1 Hybrid Reader from BioTek was used to perform the dynamic analysis. Then 200 μl of culture was loaded into each well of the 96-well plate. LB medium without cells was used as a blank. The plate was incubated at 37 °C with orbital shaking at the frequency of 807 cpm (circles per minute). Cell density (OD) of the culture was measured by absorbance at 600 nm; GFP was detected by excitation/emission at 485/515 nm. All the measurements were taken at 15- or 30-min intervals.

Estimation of the GFP-lva half-life. Plasmids carrying circuit shown in Fig. 1a were transformed into *E. coli* K-12 MG1655ΔlacIΔaraCBAD. The transformants were then grown on a LB agar plate with 100 μg/ml chloramphenicol overnight at 37 °C. In the afternoon of the second day, one colony was inoculated into 5 ml LB supplemented with 100 μg ml^{-1} chloramphenicol in a 15 ml culture and was grown overnight with 220 rotations per minute at 37 °C. In the morning of the third day, 20 μl of the overnight culture was first inoculated into 2 ml LB with 100 μg ml^{-1} chloramphenicol in a 15 ml tube and was grown to late exponential phase (OD, ~1.0; OD was measured by plate reader with 200 μl culture in one well on the 96-well plate). Then the cells were induced with 2.5×10^{-3}% L-ara for 45 min. Later, cells were washed with conditioned medium collected from overnight uninduced culture carrying the same circuit for three times and were resuspended in conditioned medium without L-ara. Last, the cell suspensions were loaded onto a 96-well plate with 200 μl per well, and OD and GFP fluorescence were measured every 15 min by the plate reader.

Microfluidics and microscopy. On day 1, plasmids carrying the SA circuit were transformed into *E. coli* K-12 MG1655ΔlacIΔaraCBAD. The transformants were then spread onto a LB agar plate with 100 μg ml^{-1} chloramphenicol and were grown at 37 °C overnight. In the morning of the second day, one colony was inoculated into 200 μl LB and were grown in a 5 ml culture tube on a shaker for about 6 h to reach the stationary phase. Then, 4 μl of the cells were inoculated into 4 ml LB medium and were grown on a shaker at 37 °C overnight using 15 ml culture tubes with or without induction. In the morning of the third day, the cells were centrifuged at 2,000*g* per 5 min followed by resuspension into 0.5 ml fresh medium with 0.75% Tween-80 (Sigma-Aldrich) and loaded onto the device. After the cells were loaded onto the device properly, fresh media with indicated induction was supplied to the cell for 16 h; then on day 4, the cells were switched to conditioned medium with indicated induction for various amounts of time as needed. Media switching was accomplished by adjusting the relative height of syringes containing fresh or conditioned medium. Details regarding the design of the chip and setup of the device can be found in ref. [50]. Phase and green fluorescent images were taken every 15 min under the magnification of ×40 with Nikon Eclipse Ti inverted microscope (Nikon) equipped with an LED-based Lumencor SOLA SE. Perfect focus was obtained automatically using Nikon Elements software. Microfluidics for the toggle switch was performed the same way with the induction switched to aTc.

Mathematical modeling. Ordinary differential equation models were developed to describe and analyze the interplay between the SA and toggle switch circuits and the host cell growth at the population level. The stochastic simulation algorithm was developed to characterize the stochastic cell division events at the single-cell level. Details are provided in the Supplementary Note.

Reporting Summary. Further information on research design is available in the Nature Research Reporting Summary linked to this article.

Data availability

All data produced or analyzed for this study are included in the published article and its supplementary information files or are available from the corresponding authors upon reasonable request.

Code availability

All the equations and parameters of the mathematical models can be found in the Supplementary Note.

References

50. Ferry, M. S., Razinkov, I. A. & Hasty, J. in *Methods in Enzymology* Vol. 497 (ed. Voigt, C.) 295–372 (Academic Press, 2011).

Acknowledgements

We thank X. Fu, T. Hong, G. Yao, J. Xing, W. Shou and T. Hwa for valuable comments. This project was supported by the ASU School of Biological and Health Systems

Engineering, NSF grant (no. EF-1921412 to X-J.T.) and NIH grant (no. GM106081 to X.W.). H.G. and J.M.-A. were also supported by the Arizona State University Dean's Fellowship.

Author contributions

X.-J.T. conceived the study. X.-J.T., R.Z. and X.W. designed the study. R.Z., J.L., P.S. and X.C. performed experiments. J.M.-A., H.G., and X.-J.T. performed model studies. R.Z., X.-J.T., Q.Z., T.D. and X.W. analyzed the data. R.Z. and X.-J.T. wrote the manuscript. H.G. and X.W. edited the manuscript.

Competing interests

The authors declare no competing interests.

Additional information

Supplementary information is available for this paper at https://doi.org/10.1038/s41589-020-0509-x.

Correspondence and requests for materials should be addressed to X.W. or X.-J.T.

Reprints and permissions information is available at www.nature.com/reprints.

nature research

Corresponding author(s): Xiaojun Tian

Last updated by author(s): Feb 4, 2020

Reporting Summary

Nature Research wishes to improve the reproducibility of the work that we publish. This form provides structure for consistency and transparency in reporting. For further information on Nature Research policies, see Authors & Referees and the Editorial Policy Checklist.

Statistics

For all statistical analyses, confirm that the following items are present in the figure legend, table legend, main text, or Methods section.

n/a	Confirmed	
☐	☒	The exact sample size (*n*) for each experimental group/condition, given as a discrete number and unit of measurement
☐	☒	A statement on whether measurements were taken from distinct samples or whether the same sample was measured repeatedly
☒	☐	The statistical test(s) used AND whether they are one- or two-sided *Only common tests should be described solely by name; describe more complex techniques in the Methods section.*
☒	☐	A description of all covariates tested
☒	☐	A description of any assumptions or corrections, such as tests of normality and adjustment for multiple comparisons
☐	☒	A full description of the statistical parameters including central tendency (e.g. means) or other basic estimates (e.g. regression coefficient) AND variation (e.g. standard deviation) or associated estimates of uncertainty (e.g. confidence intervals)
☒	☐	For null hypothesis testing, the test statistic (e.g. *F*, *t*, *r*) with confidence intervals, effect sizes, degrees of freedom and *P* value noted *Give P values as exact values whenever suitable.*
☒	☐	For Bayesian analysis, information on the choice of priors and Markov chain Monte Carlo settings
☒	☐	For hierarchical and complex designs, identification of the appropriate level for tests and full reporting of outcomes
☒	☐	Estimates of effect sizes (e.g. Cohen's *d*, Pearson's *r*), indicating how they were calculated

Our web collection on statistics for biologists contains articles on many of the points above.

Software and code

Policy information about availability of computer code

Data collection	Flow cytometry data were collected with CFlow Plus; Plate reader data were collected with Gen5 2.00; Microfluidics images were collected by NIS Elements AR4.10.01.
Data analysis	Flow cytometry data were analyzed with CFlow Plus or Matlab; Plate reader data were analyzed with Matlab.

For manuscripts utilizing custom algorithms or software that are central to the research but not yet described in published literature, software must be made available to editors/reviewers. We strongly encourage code deposition in a community repository (e.g. GitHub). See the Nature Research guidelines for submitting code & software for further information.

Data

Policy information about availability of data

All manuscripts must include a data availability statement. This statement should provide the following information, where applicable:

- Accession codes, unique identifiers, or web links for publicly available datasets
- A list of figures that have associated raw data
- A description of any restrictions on data availability

All data produced or analyzed for this study are included in the published article and its supplementary information files or are available from the corresponding author upon reasonable request.

Field-specific reporting

Please select the one below that is the best fit for your research. If you are not sure, read the appropriate sections before making your selection.

☒ Life sciences ☐ Behavioural & social sciences ☐ Ecological, evolutionary & environmental sciences

For a reference copy of the document with all sections, see nature.com/documents/nr-reporting-summary-flat.pdf

Life sciences study design

All studies must disclose on these points even when the disclosure is negative.

Sample size	3 to 6 replicates were used to generate each date point.
Data exclusions	No data was excluded. We analyzed all the generated data and presented in the text.
Replication	All attempts at replication were successful. All experiments were repeated independently at least three times, and mean ± s.d were reported.
Randomization	Each sample was started with a colony randomly picked from the corresponding culture plate.
Blinding	Yes

Reporting for specific materials, systems and methods

We require information from authors about some types of materials, experimental systems and methods used in many studies. Here, indicate whether each material, system or method listed is relevant to your study. If you are not sure if a list item applies to your research, read the appropriate section before selecting a response.

Materials & experimental systems

n/a	Involved in the study
☒	☐ Antibodies
☒	☐ Eukaryotic cell lines
☒	☐ Palaeontology
☒	☐ Animals and other organisms
☒	☐ Human research participants
☒	☐ Clinical data

Methods

n/a	Involved in the study
☒	☐ ChIP-seq
☐	☒ Flow cytometry
☒	☐ MRI-based neuroimaging

Flow Cytometry

Plots

Confirm that:

☒ The axis labels state the marker and fluorochrome used (e.g. CD4-FITC).

☒ The axis scales are clearly visible. Include numbers along axes only for bottom left plot of group (a 'group' is an analysis of identical markers).

☐ All plots are contour plots with outliers or pseudocolor plots.

☒ A numerical value for number of cells or percentage (with statistics) is provided.

Methodology

Sample preparation	All samples were diluted 5 folds with Luria-Bertani broth right before loading onto the machine.
Instrument	Accuri C6 flow cytometer from Becton Dickinson
Software	Data were collected with CFlow Plus. Percentage data were analyzed with CFlow Plus; GFP meanvalues were analyzed by Matlab.
Cell population abundance	Not applicable
Gating strategy	The boundaries between negative and positive cells were set by uninduced negative control.

☐ Tick this box to confirm that a figure exemplifying the gating strategy is provided in the Supplementary Information.